Calculations of Energy-Loss Function for 26 Materials

Yang Sun, Huan Xu, Bo Da, Shi-feng Mao, and Ze-jun Ding

Citation: Chinese Journal of Chemical Physics **29**, 663 (2016); doi: 10.1063/1674-0068/29/cjcp1605110
View online: https://doi.org/10.1063/1674-0068/29/cjcp1605110
View Table of Contents: http://cps.scitation.org/toc/cjp/29/6
Published by the American Institute of Physics

ARTICLE

Calculations of Energy-Loss Function for 26 Materials

Yang Sun, Huan Xu, Bo Da, Shi-feng Mao, Ze-jun Ding*

Hefei National Laboratory for Physical Sciences at the Microscale and Department of Physics, University of Science and Technology of China, Hefei 230026, China

(Dated: Received on May 16, 2016; Accepted on May 23, 2016)

We present a fitting calculation of energy-loss function for 26 bulk materials, including 18 pure elements (Ag, Al, Au, C, Co, Cs, Cu, Er, Fe, Ge, Mg, Mo, Nb, Ni, Pd, Pt, Si, Te) and 8 compounds (AgCl, Al_2O_3, AlAs, CdS, SiO_2, ZnS, ZnSe, ZnTe) for application to surface electron spectroscopy analysis. The experimental energy-loss function, which is derived from measured optical data, is fitted into a finite sum of formula based on the Drude-Lindhard dielectric model. By checking the oscillator strength-sum and perfect-screening-sum rules, we have validated the high accuracy of the fitting results. Furthermore, based on the fitted parameters, the simulated reflection electron energy-loss spectroscopy (REELS) spectrum shows a good agreement with experiment. The calculated fitting parameters of energy loss function are stored in an open and online database at http://micro.ustc.edu.cn/ELF/ELF.html.

Key words: Energy loss function, Dielectric function, Optical data

I. INTRODUCTION

When electrons transport in a solid, the inelastic scattering is a fundamental process. Therefore, for quantitative surface chemical analysis by surface electron spectroscopy techniques, such as X-ray photoelectron spectroscopy (XPS) and Auger electron spectroscopy (AES), the physical modeling of electron inelastic scattering is essential. The electron inelastic interaction with a sample is closely related to the energy-loss function which determines the probability of inelastic scattering event, the energy-loss distribution and the scattering angular distribution [1]. Energy-loss function, defined as $\mathrm{Im}[-1/\varepsilon(q,\omega)]$ as a function of momentum transfer $\hbar q$ and energy loss $\hbar\omega$, characterizes inelastic scattering process. The dielectric function $\varepsilon(q,\omega)$ in energy-loss function reflects the response of a solid to an external electromagnetic perturbation. As it is hard to determine q-dependent energy-loss function experimentally, Ritchie and Howie [2] suggested to derive an approximate q-dependent energy-loss function from the optical dielectric constants: by fitting the measured optical data into a finite sum of Drude-Lindhard model functions at q=0, one can extend the explicit formula to the required $\mathrm{Im}\{-1/\varepsilon(q,\omega)\}$ for finite q-values. Thus, based on the quantitative description of q-dependent energy-loss function, one can precisely study the interaction process of electrons moving in the solid by using a Monte Carlo simulations method [3]. For example, by including the surface effect on electron inelastic scattering, Ding *et al.* have successfully simulated accurate reflection electron energy-loss spectroscopy (REELS) spectra [4–7]. And the fitted energy-loss function can also be used in the calculation of surface excitation parameter [8–10].

In this work, we first briefly describe the Drude-Lindhard model of energy-loss function and the Monte Carlo method for REELS simulation. Then we present the fitting calculations of energy-loss function for 26 materials based on the experimentally measured optical data. We validate the fitting results with oscillator strength sum rule and perfect-screening-sum rule, respectively. For the application of the fitting results, one example is shown by using the fitted energy-loss function to simulate REELS spectrum and to compare with experimental measurement.

II. THEORY

A. Energy loss function

The dielectric functional theory [11] is employed to describe the electron inelastic interaction inbulk materials by:

$$\varepsilon(q,\omega) = 1 + \frac{{\omega_\mathrm{p}}^2}{{\omega_q}^2 - {\omega_\mathrm{p}}^2 - \omega\,(\omega + i\gamma)} \qquad (1)$$

where $\hbar q$ is themomentum transfer and $\hbar\omega$ is the energy loss, ω_p and γ are respectively the frequency and the damping constant of the single plasmon. ω_q denotes a

*Author to whom correspondence should be addressed. E-mail: zjding@ustc.edu.cn

dispersion relation:

$$\omega_q{}^2 = \omega_{\rm g}{}^2 + \omega_{\rm p}{}^2 + \beta^2 q^2 + \frac{q^4}{4} \tag{2}$$

where the energy $\hbar\omega_{\rm g}$ accounts for the band gap in a semiconductor.

Therefore, the bulk energy-loss function can be decomposed into N-terms of Drude-Lindhard model energy-loss function:

$$\mathrm{Im}\left[\frac{-1}{\varepsilon\left(q,\omega\right)}\right] = \sum_{i=1}^{N} a_i \mathrm{Im}\left[\frac{-1}{\varepsilon\left(q,\omega;\omega_{{\rm p}i},\gamma_i\right)}\right] \tag{3}$$

where the $3N$ parameters, a_i, $\hbar\omega_{\rm pi}$ and γ_i, are respectively the oscillator strength, energy, and width of the i-th oscillator, which are determined from an experimental optical energy-loss function (q=0) using a fitting procedure:

$$\mathrm{Im}\left[\frac{-1}{\varepsilon\left(\omega\right)}\right] = \sum_{i=1}^{N} a_i \mathrm{Im}\left[\frac{-1}{\varepsilon\left(0,\omega;\omega_{{\rm p}i},\gamma_i\right)}\right] \tag{4}$$

This implies the core electron excitations in a solid are also treated as free electrons in the spirit of a statistical model [12], and described by a Drude-Lindhard dielectric function for a plasmon pole with finite damping:

$$\begin{aligned}\varepsilon_i &= \varepsilon(q,\omega;\omega_{{\rm p}i},\gamma_i) \\ &= 1 + \frac{\omega_{{\rm p}i}{}^2}{\beta^2 q^2 + q^4/4 - \omega\left(\omega + i\gamma_i\right)}\end{aligned} \tag{5}$$

while the constant ω_g in Eq.(2) is omitted for a metal.

Thus, we can fit the optical data in the optical limit (q=0) with N-term analytic form equation:

$$\mathrm{Im}\left[\frac{-1}{\varepsilon\left(\omega\right)}\right] = \sum_{i=1}^{N} a_i \frac{\omega_{{\rm p}i}{}^2 \gamma_i \omega}{\left(\omega^2 - \omega_{{\rm p}i}{}^2\right)^2 + \left(\gamma_i\omega\right)^2} \tag{6}$$

Then according to Ritchie and Howie's scheme [2], we make an extrapolation from optical limit to other momentum transfers, and derive $\mathrm{Im}\{-1/\varepsilon\left(q,\omega\right)\}$.

B. Sum rules

We validate our fitting results with two widely used sum rules, the oscillator strength sum rule and the perfect-screening sum rule, which are limiting form of the Kramers-Kronig integral [13]. The f-sum rule is given by:

$$Z_{\rm eff} = \frac{2}{\pi\Omega_{\rm p}{}^2}\int_0^{\omega_{\max}} \omega \mathrm{Im}\left[\frac{-1}{\varepsilon\left(\omega\right)}\right]\mathrm{d}\omega \tag{7}$$

where $\hbar\Omega_{\rm p}=\sqrt{4\pi n_{\rm a}{\rm e}^2/m}$, $n_{\rm a}$ is the number density of atoms or molecules. The expectation value of $Z_{\rm eff}$ should be Z, the total number of electrons per atom or molecule for a sufficiently large value of $\omega_{\max}$.

The Kramers-Kronig relations lead to perfect-screening-sum rule given by:

$$P_{\rm eff} = \frac{2}{\pi}\int_0^{\omega_{\max}} \frac{1}{\omega}\mathrm{Im}\left[\frac{-1}{\varepsilon\left(\omega\right)}\right]\mathrm{d}\omega + \mathrm{Re}\left[\frac{1}{\varepsilon\left(0\right)}\right] \tag{8}$$

For conductors, $\mathrm{Re}[1/\varepsilon(0)]$ is zero. And in the limit $\omega_{\max}\to\infty$, the expectation value of $P_{\rm eff}$ is unity [14, 15]. For nonconductors, the refractive index n is much greater than the extinction coefficient k at low frequencies, so that $\mathrm{Re}[1/\varepsilon(0)]$ is approximately equal to $1/n^2(0)$ and Eq.(8) becomes

$$P_{\rm eff} = \frac{2}{\pi}\int_0^{\omega_{\max}} \frac{1}{\omega}\mathrm{Im}\left[\frac{-1}{\varepsilon\left(\omega\right)}\right]\mathrm{d}\omega + \frac{1}{n^2\left(0\right)} \tag{9}$$

where $n(0)$ is the limiting value of n as $\omega\to0$.

C. Monte Carlo simulation

To simulate electron scattering in a solid, we need to deal with electron elastic and inelastic scattering process. Mott's cross-section [16] is employed for the treatment of electron elastic scattering,

$$\frac{\mathrm{d}\sigma}{\mathrm{d}\Omega} = \left|f\left(\vartheta\right)\right|^2 + \left|g\left(\vartheta\right)\right|^2 \tag{10}$$

$$\begin{aligned}f(\vartheta) = \frac{1}{2ik}\sum_{l=0}^{\infty}\Big[&(l+1)\left({\rm e}^{2i\delta_l{}^+} - 1\right) + \\ &l\left({\rm e}^{2i\delta_l{}^-} - 1\right)\Big]P_l\left(\cos\vartheta\right)\end{aligned} \tag{11}$$

$$g\left(\vartheta\right) = \frac{1}{2ik}\sum_{l=1}^{\infty}\left(-{\rm e}^{2i\delta_l{}^+} + {\rm e}^{2i\delta_l{}^-}\right)P_l^1\left(\cos\vartheta\right) \tag{12}$$

where $f(\vartheta)$ and $g\left(\vartheta\right)$ the scattering amplitudes are calculated by the partial wave expansion method [17]. $P_l\left(\cos\vartheta\right)$ and $P_l^1\left(\cos\vartheta\right)$ are, respectively, the Legendre and the first-order associated Legendre function. $\delta_l{}^+$ and $\delta_l{}^-$ are spin-up and spin-down phase shifts of the l-th partial wave.

The differential inverse inelastic mean free path (DIIMFP) is represented in the dielectric theory as:

$$\frac{\mathrm{d}^2\lambda_{\rm in}^{-1}}{\mathrm{d}\left(\hbar\omega\right)\mathrm{d}q} = \frac{1}{\pi a_0 E}\mathrm{Im}\left[\frac{-1}{\varepsilon\left(q,\omega\right)}\right]\frac{1}{q} \tag{13}$$

where $\hbar\omega$ and $\hbar q$ are respectively the energy loss and the momentum transfer for an electron of kinetic energy E penetrating into a solid with dielectric function $\varepsilon(q,\omega)$. a_0 is the Bohr radius. $\lambda_{\rm in}^{-1}$ is the electron inelastic mean free path (IMFP).

We have also considered the surface electronic excitation. The surface dielectric function $\varepsilon_{\rm s}\left(\mathbf{q}_{||},\omega\right)$ is related

DOI:10.1063/1674-0068/29/cjcp1605110

with the bulk dielectric function $\varepsilon(q,\omega)$ by [5]:

$$\frac{1}{\varepsilon_s\left(\mathbf{q}_{||},\omega\right)}-2=\sum_{i=1}^{N}a_i\left[\frac{1}{\varepsilon_{si}\left(\mathbf{q}_{||},\omega\right)}-2\right] \quad (14)$$

$$\frac{1}{\varepsilon_{si}\left(\mathbf{q}_{||},\omega\right)}=1+\frac{q_{||}}{\pi}\int_{-\infty}^{\infty}\frac{\mathrm{d}q_{\perp}}{q^2\varepsilon_i\left(\mathbf{q},\omega\right)} \quad (15)$$

Based on the theory of specular surface reflection model [18, 19], we have presented the surface response function and the electron self-energy previously [5–7]. By using a vanishing surface potential and a fast-electron approximation, the random-phase-approximation self-energy of a system which is inhomogeneous in the z-direction is obtained in terms of the bulk dielectric function of solid, for the case of an electron moving toward the surface from vacuum side [20] and from the solid side [6], and for the case of an electron in the vacuum and in the solid, respectively, as follows:

$$\Sigma\left(z\,|\omega\right)=\begin{cases}\Sigma_1\left(z\,|\omega\right), & (z>0,\ \nu_{\perp}<0)\\ \Sigma_1\left(z\,|\omega\right)+\Sigma_2\left(z\,|\omega\right), & (z>0,\ \nu_{\perp}>0)\\ \Sigma_b\left(\omega\right)+\Sigma_i\left(z\,|\omega\right)+\Sigma_s\left(z\,|\omega\right)+ & \\ \quad\Sigma_{i-s}\left(z\,|\omega\right), & (z<0,\ \nu_{\perp}<0)\\ \Sigma_b\left(\omega\right)+\Sigma_i\left(z\,|\omega\right)+\Sigma_s\left(z\,|\omega\right), & \\ \qquad\qquad (z<0,\ \nu_{\perp}>0)\end{cases} \quad (16)$$

where $\Sigma_b(\omega)$, $\Sigma_i(z|\omega)$, $\Sigma_s(z|\omega)$, and $\Sigma_{i-s}(z|\omega)$ are the position-independent bulk term, the image charge term, the surface charge term, and the interference term between the image charge and the surface charge, respectively. When an electron is in vacuum region, $\Sigma_1(z|\omega)$ is the classical self-energy for an electron incident onto and escaping from the surface, and $\Sigma_2(z|\omega)$ is the extra term, which contains the contribution from both the image charge and the surface charges. Here $\nu_{\perp}$ is the vertical component of the velocity vector; the vertical distance z from the surface is positive in vacuum and negative in solid. The differential inelastic cross section near the surface, *i.e.*, the DIIMFP can be expressed in terms of the imaginary part of the different complex self-energy:

$$\sigma\left(\omega\,|E,\alpha,z\right)=-\frac{2}{\nu}\mathrm{Im}\left\{\sum\left(\omega\,|\alpha,z\right)\right\} \quad (17)$$

where α is the angle between the velocity vector and surface normal.

With the bulk- and surface-inelastic cross-section, the DIIMFP, and the Mott's elastic cross-section, we have performed Monte Carlo simulation to calculate the REELS spectrum for the considered materials. By using a Monte Carlo method [4], the flight length s between successive individual scattering events is sampled from an exponential probability distribution:

$$f\left(s\right)=\sigma\left(s\right)\exp\left\{-\int_0^s\sigma\left(s'\right)\mathrm{d}s'\right\} \quad (18)$$

where the total cross-section $\sigma(s)$ is the sum of the elastic scattering cross-section and the local inelastic cross-section. With the flight length, we can determine the next scattering event and simulate the REELS spectrum.

III. RESULTS AND DISCUSSION

As the inter-band transitions happen at the low to intermediate energy region and inner-shell ionization locates at high energy region, a wide photon energy range is necessary to fit a complete optical energy-loss function. The energy range has been shown in Table I. For most materials, we take the data from 10^{-1} eV to 10^5 eV. But some are in a smaller range due to the lack of experimental data, especially for semiconductors. The experimental data are mostly compiled in Palik's handbooks [21]. As some of the optical data are measured by different groups under different conditions, we validate the data by using the sum rules mentioned above. The selected references of each material at various energy ranges are listed in detail in Table I. We also applied a linear interpolation for the serious missing data as shown in Table I. To give an accurate fitting of these selected data, we have to use a sufficiently large number of Drude-Lindhard terms. It is obvious that the set of parameters is not unique. We also allow a negative value of a_i to reduce the number of necessary terms. The parameters of these Drude-Lindhard terms are included in a database. The full database for 26 materials is available on a website [22].

Figure 1 shows the fitting results of bulk energy-loss function $\mathrm{Im}[-1/\varepsilon(\omega)]$ for Al, Si, Fe, Mo, Ag and SiO_2 as examples. The experimental data are also shown as the references. We get a very good agreement between the fitting data and the original experimental data for both strong interband excitation and weak inner-shell ionization. For aluminum and silicon in Fig.1 (a) and (b), the strong peak near 15 eV is mainly caused by the bulk plasmon excitation. While for the three transition metals (Fe, Mo, Ag) in Fig.1 (c)−(e), the energy-loss functions are more complex due to the multiple interband transitions. Silicon oxide shown in Fig.1(f) has strong phonon excitation in very low energy near 0.1 eV. This kind of excitation is also important and cannot be neglected as the peak intensity is as strong as bulk plasmon excitation. One can always see good fitting results no matter how complex the experimental data are.

Figure 2 shows the sum-rule validation for Al, Si, and SiO_2. Eq.(9) is used for Al, while Eq.(10) for semiconductors Si and SiO_2. It also shows a good agreement between the fitting results and experimental data. As the maximum values of energy loss in each figures are above 10^4 eV, the energy range is large enough to include various excitations from all inner-shells. Note that the phonon excitation mentioned above makes a re-

DOI:10.1063/1674-0068/29/cjcp1605110

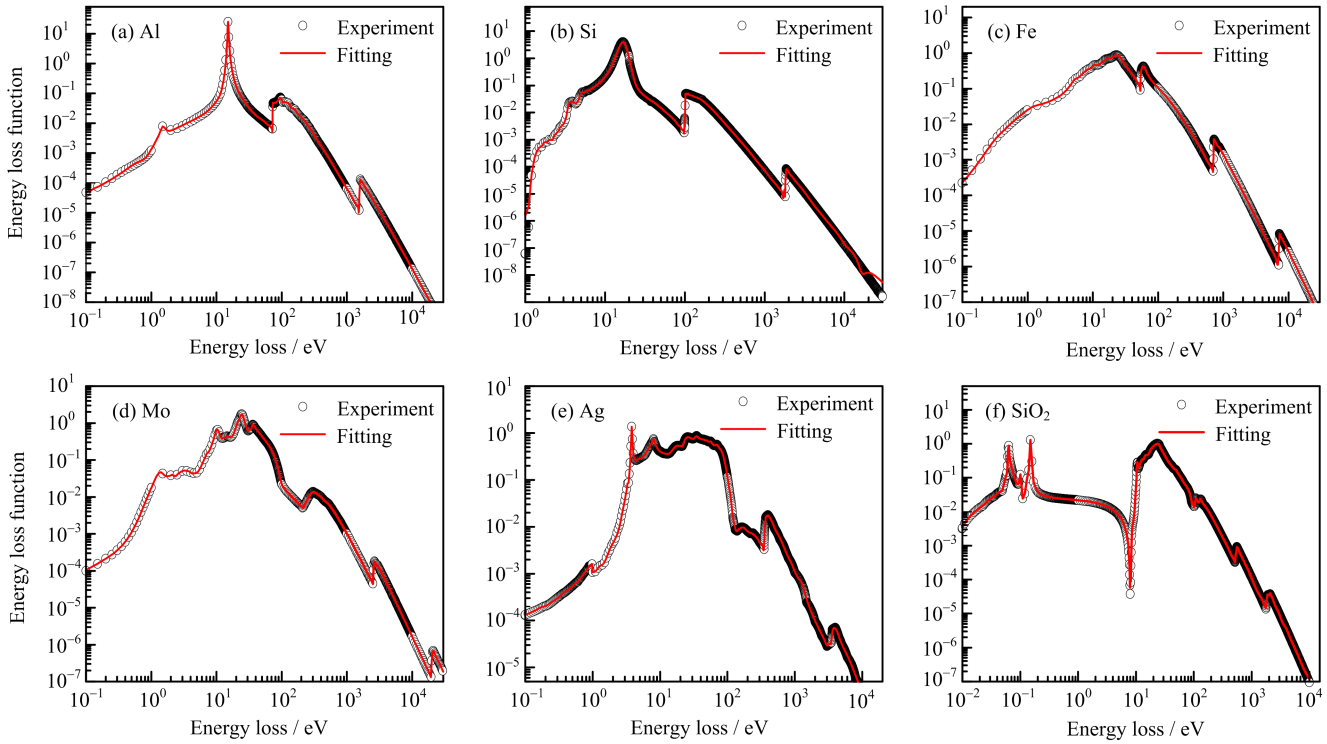

FIG. 1 The fitted bulk energy-loss function (line) and the optical bulk energy-loss function from experimental data (dot) for (a) Al, (b) Si, (c) Fe, (d) Mo, (e) Ag, and (f) SiO_2.

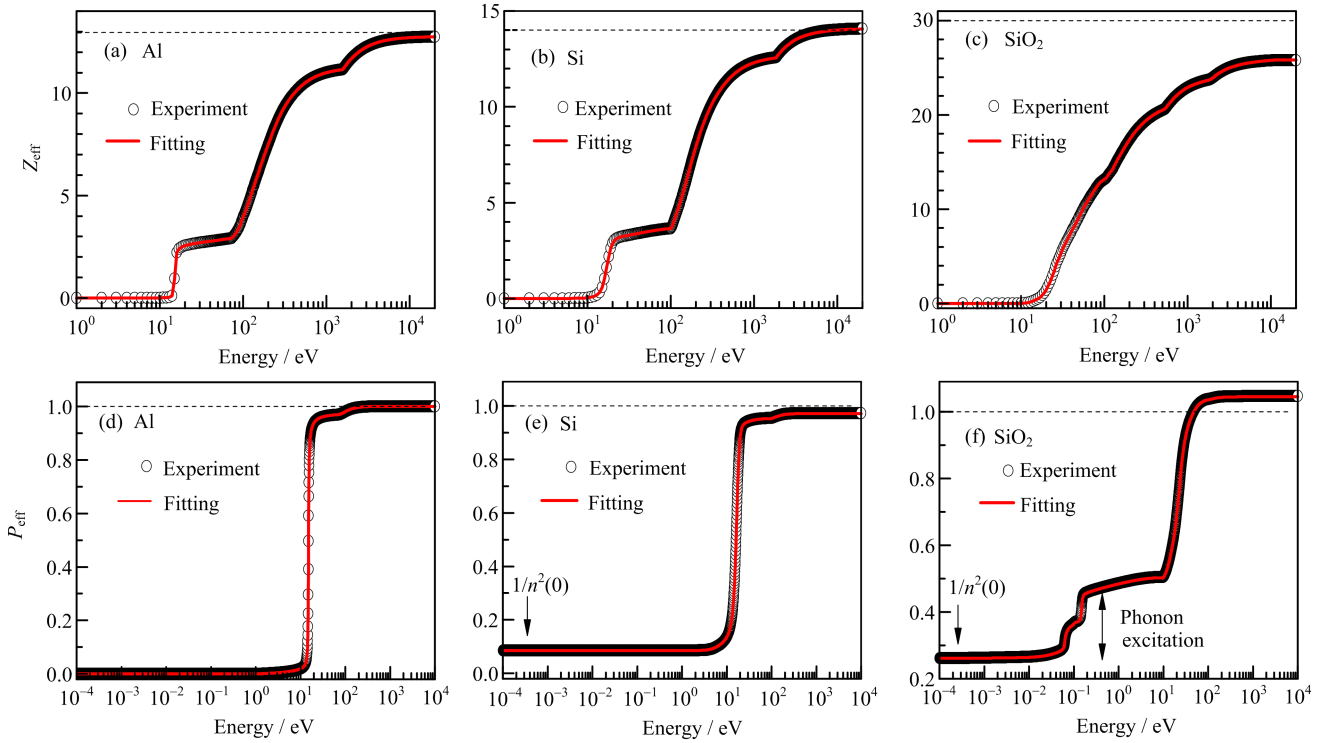

FIG. 2 The f-sum rule $Z_{\rm eff}$ and perfect-screening-sum rule $P_{\rm eff}$ for (a, d) Al, (b, e) Si, and (c, f) SiO_2. The dashed lines show the theoretical expectation value of the sum rules.

DOI:10.1063/1674-0068/29/cjcp1605110

TABLE I Sources of optical data for ELF fitting calculation.

	E/eV	Opt.	Reference		E/eV	Opt.	Reference		E/eV	Opt.	Reference
C	1−1000	n, k	[27]	Ge		k	[58]	Te	51−9988	n, k	[34]
	1000−30000	n, k	[28]		185−525	n, k	[59]	Cs	0.5−3	n, k	[92]
Mg	0.1−49990	n, k	[27]	Nb	0.1−40	n, k	[60]		3–9	n, k	[93]
Al	0.04–75	n, k	[29]		40–50	n	Interpolation		9–30	n, k	[94]
	75−30000	n, k	[28]			k	[61]		30–10000	n, k	[28]
Si	0.005–1.5	n	[30]		50–10000	n, k	[28]	AgCl	0.01–0.03	n, k	[95]
		k	[31]	Mo	0.1–60	n	[60]		0.03–1	n	[96]
	1.5–6	n, k	[32]			k	[63]			k	Interpolation
	6–20	n, k	[33]		60–100	n, k	Interpolation		1–25	n, k	[97]
	20–100	n, k	[21]		100–2000	n, k	[34]		25–1000	n, k	[98]
	100–2000	n, k	[34]		2000–10000	n, k	[28]	CdS	0.01–0.04	n	[99]
	2000–30000	n, k	[28]	Pd	0.1–0.6	n, k	[64]			k	[100]
Fe	0.01–1.2	n, k	[35]		0.6–6	n, k	[65]		0.08–1.5	n	[101]
	1.2–26	n, k	[36]		6–12	n, k	[66]			k	Interpolation
	26–10000	n, k	[37]		12–525	n, k	[67]		1.5–12	n, k	[78]
	10000–30000	n, k	[28]	AlAs	0.025–0.25	n, k	[68, 69]		37–149	n, k	[102]
Co	0.4–6.6	n, k	Interpolation		0.5–3	n	[70]		155–2000	n, k	[40]
	6.6–35.4	n, k	[38]			k	[71]	ZnSe	0.02–0.1	n, k	[74]
	38.8–200	n, k	[39]		3–5.6	n, k	[72]		0.1–2.5	n	[103]
	200–2000		[40]		51–10000	n, k	[34]			k	Interpolation
Ni	0.1–3	n, k	[41]	ZnS	0.004–0.01	n, k	[73]		2.5–10	n, k	[104]
	3–25	n, k	[42]		0.01–0.05	n, k	[74]		10–30	n, k	[105]
	25–50	n, k	[43]		0.05–2.5	n	[75]		38–150	n, k	[102]
	50–100	n, k	[44]			k	[76]		150–2000	n, k	[40]
	100–2000	n, k	[34]		2.5–80	n, k	[77, 78]	Er	0.06–2.5	n, k	[106]
	2000–10000	n, k	[45]		80–95	n, k	[21]		2.5–5.6	n, k	[107, 108]
	10000–30000	n, k	[28]		95–2000	n, k	[34]		5.6–10000	n, k	[34]
Cu	0.1–1	n, k	[46]		2000–10000	n, k	[21]	Pt	0.1–6	n, k	[109]
	1–9000	n, k	[27]	Ag	0.1–1	n, k	[46]		6–83	n, k	[110]
SiO_2	0.002–0.01	n, k	[47]		1–3	n, k	[79]		93–2000	n, k	[34]
	0.01–0.16	n, k	[48]		3–27	n, k	[80]	Au	0.1–1	n, k	[46]
	0.16–6	n	[49]		27–10000	n, k	[27]		1–6	n, k	[111]
		k	Interpolation	Al_2O_3	0.007–0.02	n, k	[81–83]		6–26	n, k	[112]
	6–25	n, k	[50]		0.02–0.12	n, k	[84]		26–88	n, k	[27]
	25–40	n, k	[21]		0.3–8	n	[85, 86]		88–10000	n	[113]
	40–150	n, k	[51]			k	Interpolation			k	[45]
	150–2000	n, k	[34]		8–42	n, k	[85, 87]	ZnTe	0.004–0.025	n, k	[74]
	2000–10000	n, k	[28]		42–118	n, k	[85]		0.025–0.8	n, k	[114]
Ge	0.002–0.018	n, k	[47]		118–142	n, k	[87]		0.8–3	n	[115]
	0.018–1	n	[52]	Te	0.001–0.06	n	[21]			k	[116]
		k	[53–55]			k	[88]		3–20	n, k	[117]
	1–6	n, k	[56]		0.06–0.3	n, k	[89]		20–100	n, k	[102]
	6–10	n, k	[57]		0.3–12	n, k	[90]		100–2000	n, k	[40]
	20–185	n	Interpolation		12–30	n, k	[91]				

markable contribution in the perfect-screening-sum rule for silicon oxide in Fig.2(f). The sum-rule validations of all the fitted material are shown in Table II. The theoretically ideal Z_{eff} should be the total number of electrons, while the ideal P_{eff} should be unity. One can see that the sum rules of fitted data are almost the same as experimental ones. However, some errors are large compared to ideal value because of the incompleteness

DOI:10.1063/1674-0068/29/cjcp1605110

TABLE II A comparison of the f-sum rule and ps-sum rule between fitting and experimental data for the 26 materials.

Element	Number of electrons	f-sum		ps-sum		Element	Number of electrons	f-sum		ps-sum	
		Optical	Fitted	Optical	Fitted			Optical	Fitted	Optical	Fitted
C	6	5.232	5.213	1.057	1.056	AlAs	46	41.075	40.748	0.471	0.469
Mg	12	15.713	15.546	1.013	1.011	ZnS	46	45.457	43.260	0.891	0.891
Al	13	12.759	12.754	1.000	1.000	Ag	47	51.759	51.152	1.152	1.152
Si	14	13.713	13.749	0.878	0.882	Al_2O_3	50	49.543	47.878	1.188	1.196
Fe	26	23.487	23.434	0.868	0.868	Te	52	62.087	61.078	1.515	1.515
Co	27	19.252	21.460	0.832	0.833	Cs	55	47.427	45.509	1.000	0.997
Ni	28	26.509	26.475	1.022	1.022	AgCl	64	56.740	59.541	0.904	0.889
Cu	29	35.640	34.114	1.001	1.001	CdS	64	30.019	29.667	0.944	0.939
SiO_2	30	25.798	25.845	1.047	1.045	ZnSe	64	50.113	49.676	0.824	0.828
Ge	32	18.874	19.148	0.694	0.693	Er	68	64.824	63.169	1.074	1.075
Nb	41	36.856	36.293	0.834	0.826	Pt	78	73.887	73.442	1.112	1.113
Mo	42	36.949	36.932	0.964	0.963	Au	79	71.786	72.236	1.091	1.091
Pd	46	31.576	31.255	1.127	1.126	ZnTe	82	63.291	62.464	0.840	0.842

and inaccuracy of the experimental data. For example, in Fig.2(f), as the optical data for silicon oxide at 0.16−6 eV are partly missing, we can see that it results in a mismatch with the expectation value. Generally, the error of Z_{eff} (from f-sum rule) is mostly caused by the incompleteness of high energy data, while the error of P_{eff} (from perfect-screening-sum rule) is caused by the incompleteness of low energy data.

With the fitted energy loss function, we can simulate REELS spectrum with a Monte Carlo method [4, 8, 23, 24]. Here we compare the simulated REELS spectrum with an experimental measurement [25, 26] for silver. The REELS spectra were measured with a cylindrical mirror analyzer (CMA) equipped with a coaxial electron gun. In this system, signal electron current was measured with a Faraday cup. The measurement was performed at a primary energy of 500 eV and for normal incidence of electrons. CMA only detects those electrons emitted from sample surface into a solid corn by the angular aperture from 36.3° to 48.3°. Hence, the Monte Carlo simulation has been performed to exactly match the experiment by counting only those reflected electrons that are detected by the CMA. Figure 3 shows the comparison between the simulation and the experiment. The inelastic scattering peaks have been normalized to the elastic peak for both simulated and experimental data. Two peaks at 4.0 and 7.4 eV correspond to surface and bulk excitation, respectively. One can see that the simulation based on the fitted energy loss function well captured both excitation phenomena and obtained a good agreement with experimental measurement.

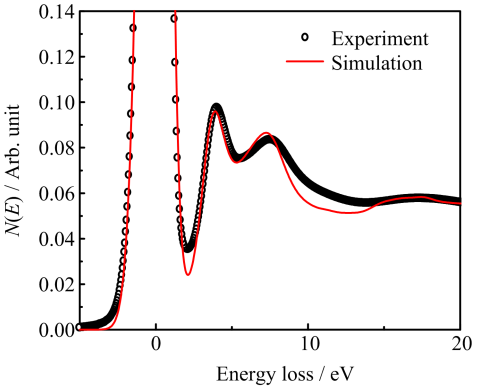

FIG. 3 The comparison of REELS spectra between the Monte Carlo simulation based on the fitted energy-loss function and the experimental measurement for silver.

IV. CONCLUSION

In summary, we have performed a systematic fitting procedure of energy-loss function for 26 materials based on the dielectric functional theory by using a finite number of Drude-Lindhard terms. We have also evaluated experimental data and fitting data with f-sum rule and perfect-screening-sum rule. It shows that the fitting procedure is accurate and the error of sum rules is mostly caused by the experimental data. The optical data are then extended to the q-dependent energy-loss function by assuming a plasmon dispersion. Thus, the surface excitation can also be described by using the derived surface dielectric function. To verify the present fitting data, we have performed a Monte Carlo simulation of the REELS spectrum for silver, and compared it with an experimental measurement. The line shapes of the simulated and experimental spectra agree with each other reasonably well for both surface and bulk features. Our fitting parameter database for energy loss function can be used in various problems of inelastic scattering in electron transport process in solids for application to surface chemical analysis by surface electron spec-

DOI:10.1063/1674-0068/29/cjcp1605110

troscopy.

V. ACKNOWLEDGMENTS

This work is supported by the National Natural Science Foundation of China (No.11274288 and No.11574289).

[1] Z. J. Ding and R. Shimizu, Scanning **18**, 92 (1996).
[2] R. H. Ritchie and A. Howie, Philos. Mag. **36**, 463 (1977).
[3] R. Shimizu and Z. J. Ding, Rep. Prog. Phys. **55**, 487 (1992).
[4] Z. J. Ding and R. Shimizu, Phys. Rev. B **61**, 14128 (2000).
[5] Z. J. Ding, Phys. Rev. B **55**, 9999 (1997).
[6] Z. J. Ding, J. Phys.: Condens. Matter **10**, 1733 (1998).
[7] Z. J. Ding, J. Phys.: Condens. Matter **10**, 1753 (1998).
[8] B. Da, S. F. Mao, G. H. Zhang, X. P. Wang, and Z. J. Ding, J. Appl. Phys. **112**, 34310 (2012).
[9] K. Salma, Z. J. Ding, H. M. Li, and Z. M. Zhang, Surf. Sci. **600**, 1526 (2006).
[10] K. Salma, Z. J. Ding, Z. M. Zhang, P. Zhang, K. Tokesi, D. Varga, and J. Toth, Surf. Sci. **603**, 1236 (2009).
[11] P. M. Echenique, R. H. Ritchie, and W. Brandt, Phys. Rev. B **20**, 2567 (1979).
[12] C. J. Tung, J. C. Ashley, and R. H. Ritchie, Surf. Sci. **81**, 427 (1979).
[13] S. Tanuma, C. J. Powell, and D. R. Penn, J. Electron Spectrosc. Relat. Phenom. **62**, 95 (1993).
[14] P. Nozieres and D. Pines, *Theory Of Quantum Liquids*, Boulder: Westview Press, (1999).
[15] G. D. Mahan, *Many-Particle Physics*, 3rd ed., New York: Springer, (2013).
[16] N. F. Mott, Proc. R. Soc. London A **124**, 425 (1929).
[17] Y. Yamazaki, *Ph. D. Dissertation*, Osaka: Osaka University, (1977).
[18] R. A. Bonham and T. G. Strand, J. Chem. Phys. **39**, 2200 (1963).
[19] R. H. Ritchie and A. L. Marusak, Surf. Sci. **4**, 234 (1966).
[20] F. Flores and F. Garcia-Moliner, J. Phys. C **12**, 907 (1979).
[21] E. D. Palik, *Handbook of Optical Constants of Solids*, 3rd ed., Cambridge: Academic Press, (1998).
[22] http://micro.ustc.edu.cn/ELF/ELF.html.
[23] Z. J. Ding, H. M. Li, Q. R. Pu, Z. M. Zhang, and R. Shimizu, Phys. Rev. B **66**, 85411 (2002).
[24] B. Da, S. F. Mao, and Z. J. Ding, J. Phys.: Condens. Matter **23**, 395003 (2011).
[25] K. Goto, N. Sakakibara, Y. Takeichi, Y. Numata, and Y. Sakai, Surf. Interface Anal. **22**, 75 (1994).
[26] Y. Takeichi and K. Goto, Surf. Interface Anal. **25**, 17 (1997).
[27] H. J. Hagemann, W. Gudat, and C. Kunz, J. Opt. Soc. Am. **65**, 742 (1975).
[28] B. L. Henke, E. M. Gullikson, and J. C. Davis, At. Data Nucl. Data Tables **54**, 181 (1993).
[29] E. Shiles, T. Sasaki, M. Inokuti, and D. Y. Smith, Phys. Rev. B **22**, 1612 (1980).
[30] H. H. Li, J. Phys. Chem. Ref. Data **9**, 561 (1980).
[31] B. Bendow, H. G. Lipson, and S. P. Yukon, Appl. Opt. **16**, 2909 (1977).
[32] D. E. Aspnes and J. B. Theeten, J. Electrochem. Soc. **127**, 1359 (1980).
[33] H. R. Philipp, J. Appl. Phys. **43**, 2835 (1972).
[34] B. L. Henke, P. Lee, T. J. Tanaka, R. L. Shimabukuro, and B. K. Fujikawa, At. Data Nucl. Data Tables **27**, 1 (1982).
[35] M. A. Ordal, R. J. Bell, R. W. Alexander, L. L. Long, and M. R. Querry, Appl. Opt. **24**, 4493 (1985).
[36] T. J. Moravec, J. C. Rife, and R. N. Dexter, Phys. Rev. B **13**, 3297 (1976).
[37] V. M. Shirokovskii, M. M. Kirillova, and N. A. Shilkova, Sov. Phys. JEPT **55**, 463 (1982).
[38] C. Werenkel and B. Gauthé, Phys. Status Solidi **64**, 515 (1974).
[39] B. Sonntag, R. Haensel, and C. Kunz, Solid State Commun. **7**, 597 (1969).
[40] B. L. Henke, Am. Inst. Phys. Conf. Proc. **75**, 146 (1981).
[41] D. W. Lynch, R. Rosei, and J. H. Weaver, Solid State Commun. **9**, 2195 (1971).
[42] R. C. Vehse and E. T. Arakawa, Phys. Rev. **180**, 695 (1969).
[43] J. H. Weaver, C. Krafka, D. W. Lynch, and E. E. Koch, Appl. Opt. **20**, 1124 (1981).
[44] L. A. Feldkamp, M. B. Stearns, and S. S. Shinozaki, Phys. Rev. B **20**, 1310 (1979).
[45] M. V Zombeck, G. K. Austin, and D. T. Torgerson, *Smithsonian Astrophysical Observatory Report SAO-AXAF-80-003*, Appendix B, Table B1, Massachusetts, Cambridge: Smithsonian Astrophysical Observatory, (1980).
[46] B. Dold and R. Mecke, Optik **22**, 435 (1965).
[47] C. M. Randall and R. D. Rawcliffe, Appl. Opt. **6**, 1889 (1967).
[48] H. R. Philipp, J. Appl. Phys. **50**, 1053 (1979).
[49] B. Brixner, J. Opt. Soc. Am. **57**, 674 (1967).
[50] H. R. Philipp, Solid State Commun. **4**, 73 (1966).
[51] J. Rife and J. Osantowski, J. Opt. Soc. Am. **70**, 1513 (1980).
[52] N. P. Barnes and M. S. Piltch, J. Opt. Soc. Am. **69**, 178 (1979).
[53] R. J. Collins and H. Y. Fan, Phys. Rev. **93**, 674 (1954).
[54] D. L. Stierwalt and R. F. Potter, in *Proceedings of the International Conference on the Physics of Semiconductors*, A. C. Stickland Ed., London: The Institute of Physics and The Physical Society, 513 (1962).
[55] W. C. Dash and R. Newman, Phys. Rev. **99**, 1151 (1955).
[56] D. E. Aspnes and A. A. Studna, Phys. Rev. B **27**, 985 (1983).
[57] H. R. Philipp and E. A. Taft, Phys. Rev. **113**, 1002 (1959).
[58] M. Cardona, W. Gudat, B. Sonntag, and P. Y. Yu, *in Proceedings of the International Conference on the Physics of Semiconductors*, S. P. Keller, J. C. Hensel, and F. Stern, Eds., Springfield: U. S. AEC Division of Technical Information, 208 (1970).
[59] A. P. Lukirskii, E. P. Savinov, O. A. Ershov, and Y.

DOI:10.1063/1674-0068/29/cjcp1605110

F. Shepelev, Opt. Spectrosc. **16**, 168 (1964).
[60] J. H. Weaver, D. W. Lynch, and C. G. Olson, Phys. Rev. B **7**, 4311 (1973).
[61] J. H. Weaver and C. G. Olson, Phys. Rev. B **14**, 3251 (1976).
[62] J. Weaver, D. W. Lynch, and C. G. Olson, Phys. Rev. B **10**, 501 (1974).
[63] D. W. Juenker, L. J. LeBlanc, and C. R. Martin, J. Opt. Soc. Am. **58**, 164 (1968).
[64] O. S. Heavens, *Optical Properties of Thin Solid Films*, New York: Dover, (1965).
[65] P. B. Johnson and R. W. Christy, Phys. Rev. B **9**, 5056 (1974).
[66] R. C. Vehse, E. T. Arakawa, and M. W. Williams, Phys. Rev. B **1**, 517 (1970).
[67] D. L. Windt, W. C. Cash, M. Scott, P. Arendt, B. Newnam, R. F. Fisher, and A. B. Swartzlander, Appl. Opt. **27**, 246 (1988).
[68] S. Perkowitz, R. Sudharsanan, S. S. Yom, and T. J. Drummond, Solid State Commun. **62**, 645 (1987).
[69] R. Sudharsanan, S. Perkowitz, S. S. Yom, and T. J. Drummond, Proc. SPIE **794**, 197 (1987).
[70] S. Adachi, J. Appl. Phys. **58**, R1 (1985).
[71] W. M. Yim, J. Appl. Phys. **42**, 2854 (1971).
[72] M. Garriga, P. Lautenschlager, M. Cardona, and K. Ploog, Solid State Commun. **61**, 157 (1987).
[73] T. Hattori, Y. Homma, A. Mitsuishi, and M. Tacke, Opt. Commun. **7**, 229 (1973).
[74] A. Manabe, A. Mitsuishi, and H. Yoshinaga, Jpn. J. Appl. Phys. **6**, 593 (1967).
[75] A. N. Pikhtin and A. D. Yas'kov, Sov. Phys. Semicond. **12**, 622 (1978).
[76] S. J. Czyzak, D. C. Reynolds, R. C. Allen, and C. C. Reynolds, J. Opt. Soc. Am. **44**, 864 (1954).
[77] W. R. Hunter, D. W. Angel, and G. Hass, J. Opt. Soc. Am. **68**, 1319 (1978).
[78] M. Cardona and G. Harbeke, Phys. Rev. **137**, A1467 (1965).
[79] P. Winsemius, F. F. Van Kampen, H. P. Lengkeek, and C. G. Van Went, J. Phys. F **6**, 1583 (1976).
[80] G. Leveque, C. G. Olson, and D. W. Lynch, Phys. Rev. B **27**, 4654 (1983).
[81] E. E. Russell and E. E. Bell, J. Opt. Soc. Am. **57**, 543 (1967).
[82] E. V. Loewenstein, D. R. Smith, and R. L. Morgan, Appl. Opt. **12**, 398 (1973).
[83] W. B. Cook and S. Perkowitz, Appl. Opt. **24**, 1773 (1985).
[84] F. Gervais and B. Piriou, J. Phys. C **7**, 2374 (1974).
[85] T. Tomiki, Y. Ganaha, T. Futemma, T. Shikenbaru, Y. Aiura, M. Yuri, S. Sato, H. Fukutani, H. Kato, T. Miyahara, J. Tamashiro, and A. Yonesu, J. Phys. Soc. Jpn **62**, 1372 (1993).
[86] M. A. Jeppesen, J. Opt. Soc. Am. **48**, 629 (1958).
[87] R. H. French, H. Mllejans, and D. J. Jones, J. Am. Ceram. Soc. **81**, 2549 (1998).
[88] R. Geick, P. Grosse, and W. Richter, *Physics of Selenium and Tellurium*, New York: Pergamon, (1969).
[89] R. S. Caldwell and H. Y. Fan, Phys. Rev. **114**, 664 (1959).
[90] S. Tutihasi, G. G. Roberts, R. C. Keezer and R. E. Drews, Phys. Rev. **177**, 1143 (1969).
[91] P. Bammes, R. Klucker, E. E. Koch, and T. Tuomi, Phys. Status Solidi **49**, 561 (1972).
[92] N. V. Smith, Phys. Rev. B **2**, 2840 (1970).
[93] U. S. Whang, E. T. Arakawa, and T. A. Callcott, J. Opt. Soc. Am. **61**, 740 (1971).
[94] S. Sato, T. Miyahara, T. Hanyu, S. Yamaguchi, and T. Ishii, J. Phys. Soc. Jpn **47**, 836 (1979).
[95] A. Hadni, J. Claudel, and P. Strimer, Appl. Opt. **7**, 1159 (1968).
[96] L. W. Tilton, E. K. Plyler, and R. E. Stephens, J. Opt. Soc. Am. **40**, 540 (1950).
[97] R. S. Bauer, W. E. Spicer, and J. J. White III, J. Opt. Soc. Am. **64**, 830 (1974).
[98] N. J. Carrera and F. C. Brown, Phys. Rev. B **4**, 3651 (1971).
[99] M. Balkanski, *in Optical Properties of Solids*, F. Abelès Ed., Amsterdam: North-Holland Pub. Co., 529 (1972).
[100] M. Balkanski, J. M. Besson, and R. Le Toullec, *in Proceedings of the International Conference on the Physics of Semiconductors*, M. Hulin Ed., New York: Academic, 1091 (1964).
[101] A. B. Francis and A. I. Carlson, J. Opt. Soc. Am. **50**, 118 (1960).
[102] M. Cardona and R. Haensel, Phys. Rev. B **1**, 2605 (1970).
[103] A. Feldman, I. H. Malitson, D. Horwitz, R. M. Waxler, and M. J. Dodge, Natl. Bur. Stand. (U.S.), Tech. Note **993**, 63 (1979).
[104] M. Balkanski and Y. Petroff, *in Proceedings of the International Conference on the Physics of Semiconductors*, M. Hulin Ed., New York: Academic, 245 (1964).
[105] J. Gautron, C. Raisin, and P. Lemasson, J. Phys. D **15**, 153 (1982).
[106] Y. V. Knyazev and M. M. Noskov, Sov. J. Low Temp. Phys. **4**, 376 (1978).
[107] J. H. Weaver and D. W. Lynch, Phys. Rev. Lett. **34**, 1324 (1975).
[108] Y. V. Knyazev and G. A. Bolotin, Phys. Met. Metallogr. **61**, 57 (1986).
[109] J. H. Weaver, Phys. Rev. B **11**, 1416 (1975).
[110] W. R. Hunter, D. W. Angel, and G. Hass, J. Opt. Soc. Am. **69**, 1695 (1979).
[111] M. L. Thèye, Phys. Rev. B **2**, 3060 (1970).
[112] L. R. Canfield, G. Hass, and W. R. Hunter, J. Phys. **25**, 124 (1964).
[113] P. O. Nilsson, Phys. Kondens. Mater. **11**, 1 (1970).
[114] R. E. Nahory and H. Y. Fan, Phys. Rev. **156**, 825 (1967).
[115] T. R. Sliker and J. M. Jost, J. Opt. Soc. Am. **56**, 130 (1966).
[116] G. A. Zholkevich, Sov. Phys. Solid State **2**, 1009 (1960).
[117] M. Cardona, J. Appl. Phys. **36**, 2181 (1965).

DOI:10.1063/1674-0068/29/cjcp1605110